

Dephasing of qubits by transverse low-frequency noise

Yu. Makhlin^{+,*1)} and A. Shnirman⁺

⁺Institut für Theoretische Festkörperphysik, Universität Karlsruhe, D-76128 Karlsruhe, Germany

^{*}L. D. Landau Institute for Theoretical Physics RAS, 117940 Moscow, Russia

Submitted 23 September 2003

We analyze the dissipative dynamics of a two-level quantum system subject to low-frequency, e.g. $1/f$ noise, motivated by recent experiments with superconducting quantum circuits. We show that the effect of transverse linear coupling of the system to low-frequency noise is equivalent to that of quadratic longitudinal coupling. We further find the decay law of quantum coherent oscillations under the influence of both low- and high-frequency fluctuations, in particular, for the case of comparable rates of relaxation and pure dephasing.

PACS: 03.65.Yz, 75.10.Jm, 85.25.Cp

Recent experiments with superconducting Josephson-junction circuits [1, 2] demonstrated quantum coherent oscillations with a long decay time and a quality factor up to $\sim 10^4$. These experiments, on one hand, probe coherent properties of Josephson qubits (quantum bits) and demonstrate their potential for applications in quantum computing and quantum communication. On the other hand, they may be viewed as a probe of the noise mechanisms in the devices studied.

For the description of the dynamics of a two-level system (qubit, spin) subject to weak short-correlated noise one may use the Bloch equation, known from the NMR studies, which describes exponential relaxation of the longitudinal spin component and dephasing of the precessing transverse spin component (here and below we use the spin-1/2 language to discuss the dynamics). This description is valid as long as the correlation time of the noise is short compared to the typical dissipative times T_1, T_2 . However, in Josephson-junction qubits the low-frequency noise is strong. These low-frequency fluctuations are correlated over distant times, and special treatment of their influence on a qubit is needed. They could lead to complicated decay laws [3–6]. In Ref. [7] the influence of low-frequency fluctuations nonlinearly coupled to a qubit was analyzed; this analysis is relevant for operation at the so-called optimal operation points [1]. Here we extend this analysis to account for the effect of transverse fluctuations also present at optimal points. While our discussion applies to an arbitrary dissipative two-level system, for illustration we consider the Josephson charge qubit, similar to that studied in the experiment [1]. We begin by discussing this system

and the relevant noise sources and then proceed to the analysis of dephasing in general and at optimal points.

Dissipative dynamics of a Josephson charge qubit. The simplest Josephson charge qubit is the Cooper-pair box shown in Fig.1 [8]. It consists of a su-

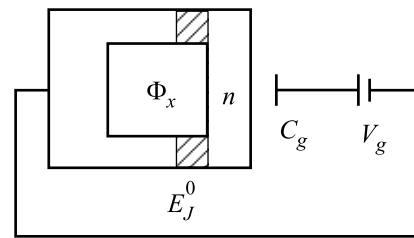


Fig.1. The simplest Josephson charge qubit

perconducting island connected by a dc-SQUID (effectively, a Josephson junction with the coupling $E_J(\Phi_x) = 2E_J^0 \cos(\pi\Phi_x/\Phi_0)$ tunable via the magnetic flux Φ_x ; here $\Phi_0 = hc/2e$) to a superconducting lead and biased by a gate voltage V_g via a gate capacitor C_g . The Josephson energy of the junctions in the SQUID loop is E_J^0 , and their capacitance C_J^0 sets the charging-energy scale $E_C \equiv e^2/2(C_g + C_J)$, $C_J = 2C_J^0$. At low enough temperatures single-electron tunneling is suppressed and only even-parity states are involved. Here we consider low-capacitance junctions with high charging energy $E_C \gg E_J^0$. Then the number n of Cooper pairs on the island (relative to a neutral state) is a good quantum number; at certain values of the bias $V_g \approx V_{\text{deg}} = (2n+1)e/C$ two lowest charge states n and $n+1$ are near-degenerate, and even a weak E_J mixes them strongly. At low temperatures and operation frequencies higher charge states do

¹⁾e-mail: makhlin,shnirman@tfp.uni-karlsruhe.de

not play a role. The Hamiltonian reduces to a two-state model,

$$\mathcal{H} = -\frac{1}{2}[E_{\text{ch}}(V_g)\hat{\sigma}_z + E_J(\Phi_x)\hat{\sigma}_x], \quad (1)$$

in the basis $|\downarrow\rangle = |n\rangle$, $|\uparrow\rangle = |n+1\rangle$; here $E_{\text{ch}}(V_g) = 2e(V_g - V_{\text{deg}})C_g/(C_J + C_g)$. The Hamiltonian (1) can be controlled via the gate voltage V_g and the applied flux Φ_x , this allows one to manipulate the qubit's state and perform quantum logic operations. To read out the final quantum state one has to couple the qubit to a quantum detector, e.g. a single-electron transistor [8].

Quantum bits are inevitably coupled to fluctuations in the environment (bath). This destroys the coherence of the qubits' dynamics. To slow down the dephasing the coupling should be made as weak as possible. In solid-state systems decoherence is potentially strong due to numerous microscopic modes. In Josephson qubits the noise is dominated by material-dependent sources, such as background-charge fluctuations or variations of magnetic fields and critical currents, with power spectrum peaked at low frequencies, often $1/f$. A further relevant contribution is the electromagnetic noise of the control circuit, typically Ohmic at low frequencies. The $1/f$ noise appears difficult to suppress and, since the dephasing is dominated by low-frequency noise, it is particularly destructive. On the other hand, Vion et al. [1] showed that the effect of this noise can be substantially reduced by tuning the linear longitudinal qubit-noise coupling to zero (in a modified design; they also suppressed the coupling to the quantum detector to minimize its effect on the qubit before the read-out). This increased the coherence time by 2–3 orders of magnitude compared to earlier experiments.

Of special interest is the analysis of the slow dephasing at such an optimal point. On one hand, comparison of theory and experiment may verify our understanding of the physics of the device studied as a dissipative two-level system. Further, from the analysis of the dephasing time scale and the decay law one may extract additional information about the statistical properties of the noise. On the other hand, understanding of the dissipative processes should allow their further suppression in future qubit designs.

Part of the noise (including the background-charge fluctuations) can be thought of as fluctuations of the gate voltage and another part as fluctuations of the control flux Φ_x . It is convenient to discuss the effect of, e.g., the voltage noise $V_g = V_g^0 + Y(t)$ in the qubit's eigenbasis:

$$\mathcal{H} = -\frac{1}{2}[\Delta E \hat{\sigma}_z + \zeta \hat{Y}(t)(-\sin \eta \hat{\sigma}_x + \cos \eta \hat{\sigma}_z)], \quad (2)$$

where the level splitting $\Delta E = (E_{\text{ch}}(V_g^0)^2 + E_J^2)^{1/2}$ and the angle between the static and fluctuating 'magnetic' fields is given by $\tan \eta = E_J/E_{\text{ch}}(V_g^0)$. We expanded the variation of E_{ch} in Y to the linear order. Consider first the effect of weak short-correlated noise (with correlation time shorter than the dissipative times; this includes the finite-temperature Ohmic noise). In this case one can use the lowest-order perturbation theory and finds that the spin dynamics is described by the Bloch equations, known from NMR. The interlevel transitions are induced by the *transverse* fluctuations $\propto \sin \eta$ and give the relaxation time $1/T_1 = \zeta^2 \sin^2 \eta S_Y(\omega = \Delta E)/2$; the dephasing time is $1/T_2 = 1/2T_1 + 1/T_2^*$, where the pure dephasing is induced by the *longitudinal* noise $\propto \cos \eta$ and gives $1/T_2^* = \zeta^2 \cos^2 \eta S_Y(\omega = 0)/2$ (here the noise power $S_Y(t) = (1/2)\langle [Y(t), Y(0)]_+ \rangle$; we set $\hbar = 1$). The effect of the magnetic-flux noise can be analyzed similarly. For Josephson qubits these expressions give good estimates for the measured relaxation times but do not suffice to describe the dephasing. Indeed, the expression for T_2^* cannot be used for strong longitudinal low-frequency, e.g. $1/f$ noise; still it indicates that dephasing is strong. In first experiments [9, 4] dephasing times in the range of fractions to a few nanoseconds were achieved. Tuning to an optimal point extended the coherence time to $\sim 1 \mu\text{s}$ [1].

Dephasing at optimal point. We illustrate our discussion of decoherence at an optimal point by considering a qubit deep in the charge limit, although in the device of Ref. [1] E_C and E_J were comparable (in which case two lowest eigenstates, which form the qubit, are no longer charge states). Using two control parameters V_g and Φ_x one can tune the longitudinal linear couplings to the charge and flux noise to zero: For instance, for the system (2) tuning the gate voltage to the degeneracy point $E_{\text{ch}}(V_g^0) = 0$ yields $\cos \eta = 0$. Further, tuning Φ_x to the point of maximal $E_J(\Phi_x)$ also suppresses the linear coupling to the flux fluctuations $\Phi_x = \Phi_x^0 + X(t)$. Thus, at this optimal point the Hamiltonian reads:

$$\mathcal{H} = -\frac{1}{2}[\Delta E \hat{\sigma}_z + \lambda X^2 \hat{\sigma}_z + \zeta Y \hat{\sigma}_x], \quad (3)$$

where we left only the leading fluctuating terms.

The quadratic longitudinal low-frequency noise $\lambda X^2 \hat{\sigma}_z$ may result in an unusual dephasing law (with a power law crossing over to exponential decay) due to strong higher-order contributions [7]. Here we discuss the effect of the transverse noise $\zeta Y \hat{\sigma}_x$. It can lead to relaxation processes and contribute to pure dephasing in higher orders. Thus in the analysis of dephasing one needs to account for both λX^2 and ζY terms.

The effect of the low-frequency ($\omega \ll \Delta E$) transverse noise can be treated in the adiabatic approximation: we diagonalize (3) to $-\hat{\sigma}_z \sqrt{(\Delta E + \lambda X^2)^2 + (\zeta Y)^2}/2 \approx -\hat{\sigma}_z [\Delta E + \lambda X^2 + \zeta^2 Y^2/(2\Delta E)]/2$, thus the low- ω transverse noise contributes to pure dephasing. In general higher-frequency fluctuations are also present and induce relaxation. If the relaxation is much slower than the pure dephasing, one may neglect its contribution to the total dephasing. If the relaxation is much faster, it dominates the decoherence; in this limit its rate $\zeta^2 S_Y(\Delta E)/2$ is given by the golden rule. However, of special experimental interest [1] is the situation with comparable relaxation and pure-dephasing time scales. We analyze whether evaluation of each of them is influenced by the other in this case, that is whether the low- and high- ω contributions interfere. In particular, we expect [7] strong higher-order contributions to the pure dephasing due to strong low- ω noise. Does it also contribute to relaxation? In the lowest order the relaxation is due to transitions with emission of a single resonant bath excitation; can instead a near-resonant excitation be emitted accompanied by low-frequency excitations? Here we show how the dephasing and relaxation laws and time scales can be obtained.

Dephasing by transverse noise. We begin with a discussion of purely transverse noise, $\lambda = 0$. We focus on the long-correlated noise (slow decay of $\langle Y(0)Y(t) \rangle$), i.e. on the noise power peaked at low and smooth at high frequencies. In our analysis below we assume weak dissipation: pure dephasing and relaxation slower than the oscillations, $\Gamma \ll \Delta E$, where Γ represents the total-dephasing time scale. This limit is of primary interest for the circuits that realize qubits. Further, below for illustration we consider a source of Gaussian noise $Y(t)$, which can be characterized by its second correlator, but our major conclusions persist in more general situations.

Our discussion is based on the analysis of the evolution operator of the qubit dynamics using the ‘real-time’ Keldysh diagrammatic expansion in the qubit-bath coupling (this approach [10] is useful, since the spin degree of freedom does not satisfy the Wick theorem; it reminds the approach of Ref. [11]). We begin by showing that the subleading-order effects of the low-frequency transverse noise reduce to the lowest-order contribution of longitudinal quadratic noise (this can also be seen from the adiabatic approximation but our derivation indicates the diagrams, important in the discussion below).

In the diagrams the horizontal direction explicitly represents the time axis. The solid lines describe the unperturbed (here, coherent) evolution of the qubit’s 2×2 density matrix $\hat{\rho}$, $\exp(-iL_0 t)\theta(t)$, where L_0 is the bare Liouville operator (this translates to $1/(\omega - iL_0)$ in

the frequency domain). The vertices are explicitly time-ordered; each of them contributes the term $\zeta Y \sigma_x \tau_z/2$, with the bath operator $Y(t)$ and the Keldysh matrix $\tau_z = \pm 1$ for vertices on the upper/lower time branch. Averaging over the fluctuations should be performed; for Gaussian correlations it pairs the vertices as indicated by dashed lines in Fig.2, each of the lines corresponding to a correlator $\langle YY \rangle$. Fig.2 shows contributions to

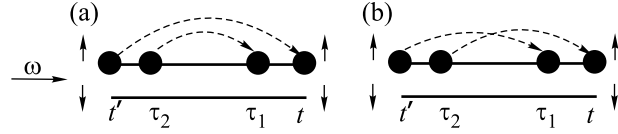


Fig.2. Second-order contributions to the self-energy $\Sigma_{\uparrow\downarrow\leftarrow\uparrow\downarrow}$. Other terms are obtained by shifting an even number of the vertices in (a) or (b) to the lower branch

the second-order self-energy $\Sigma_{\uparrow\downarrow\leftarrow\uparrow\downarrow}^{(2)}$ (here $ij = \uparrow\downarrow$ label four entries of the qubit’s density matrix). The term in Fig.2a gives

$$\left(\frac{\zeta}{2}\right)^4 \int d\tau_1 d\tau_2 \langle Y(t)Y(t') \rangle \langle Y(\tau_1)Y(\tau_2) \rangle e^{i\Delta E(\tau_1 - \tau_2)}, \quad (4)$$

with integration over the domain $t' < \tau_2 < \tau_1 < t$.

After the summation over vertex positions on the lower/upper branches in Figs.2a,b, we evaluate the behavior of the Fourier-transformed self-energy in the vicinity of the level splitting, at $\omega = -\Delta E - \omega' + i0$, where $\omega' \ll \Delta E$. If the integral is dominated by low frequencies, we find:

$$\begin{aligned} \text{Re } \Sigma_{\uparrow\downarrow\leftarrow\uparrow\downarrow}^{(2)}(\omega = -\Delta E - \omega' + i0) &\approx -\frac{\zeta^4}{8\Delta E^2} \int \frac{d\nu}{2\pi} \times \\ &\times [\langle Y_{\nu+\omega'}^2 \rangle \langle Y_{-\nu}^2 \rangle + \langle Y_{\nu-\omega'}^2 \rangle \langle Y_{-\nu}^2 \rangle] = -\frac{1}{2} S_{Y_2}(\omega'), \end{aligned} \quad (5)$$

where S_{Y_2} is the noise of

$$Y_2 \equiv \zeta^2 Y^2 / (2\Delta E). \quad (6)$$

The result (5) coincides, as expected, with the lowest-order contribution of the term $-Y_2 \sigma_z/2$; note that the left and right vertex pairs in Fig.2 can be viewed as composite vertices corresponding to $-Y_2 \sigma_z/2$. Below we demonstrate that similar reduction occurs in every order of the perturbative expansion. Specifically, we show that the decay of the off-diagonal entry of the density matrix is $\rho_{\uparrow\downarrow}(t) = \rho_{\uparrow\downarrow}(0) \cdot \exp(-t/2T_1) \cdot \gamma_\varphi(t)$, where the relaxation time is given by the golden rule and the pure dephasing term $\gamma_\varphi(t)$ is the same as for the longitudinal fluctuations $-Y_2 \sigma_z/2$ (analyzed in Ref. [7]).

To demonstrate this we consider the diagrammatic calculation of the evolution operator for the density matrix. We begin by evaluating the evolution of the off-diagonal entry $\rho_{\uparrow\downarrow}^{\dagger}$ (the phase dynamics and dephasing), and then discuss relaxation (evolution of $\rho_{\uparrow\uparrow}^{\dagger}, \rho_{\downarrow\downarrow}^{\dagger}$).

The expansion of the propagator contains vertices on the horizontal solid lines, representing the Keldysh contour. For a given number and ordering of the vertices, one is to integrate over their time positions, and then add up all diagrams. Consider the dependence of the integrand on the time position of a vertex. This dependence includes fast oscillations with frequency $\pm\Delta E$, since the vertex flips the spin and changes the energy of the bare hamiltonian $-\Delta E \sigma_z/2$, and a much slower dependence of the dashed line. Thus the integrand is a fast oscillating function of the time positions of each vertex. Since integration is typically performed over time range much wider than the period of oscillations (at all times of interest for the analysis of dephasing; this range is $\sim 1/\Gamma$ at $t \sim 1/\Gamma$), the contribution of the most part of the integration space (with vertices' time positions as coordinates) is strongly suppressed by fast oscillations. However, in certain directions in this space, in which pairs of vertices with opposite oscillation frequencies $\pm\Delta E$ move together, the variation is slow, and the respective domains dominate the integral. One can arrive at this conclusion, and determine the dominant domains, by considering the evaluation of a particular diagram: the integral over the time t of a vertex $\int_a^b g(t) \exp(i\Delta Et) dt$ is taken between the positions a, b of the neighboring vertices. Since $g(t)$ is slow on scale $1/\Delta E$, the oscillatory integral is dominated by the boundary terms, $g(t) \exp(i\Delta Et)|_a^b / i\Delta E$. One can say that the vertex t joins one of its neighbors, and later one integrates over the vertex-pair position, a or b .

One can continue this process, integrating at each step over time positions of unpaired vertices (or clusters with an odd number of vertices and hence oscillatory behavior), if any are still present. Finally one arrives at a situation where all vertices are paired, and the dependence of the integrand on pair time positions is slow (the exponentials $\exp(\pm i\Delta Et)$ for two paired vertices compensate each other). The integral in each domain with a fixed time ordering is dominated by the boundary terms, that is the terms with paired vertices. Thus we eliminate the high-frequency ($\sim \Delta E$) behavior, and now can evaluate the propagators using the diagram technique with ingredients that are slow (without oscillatory dependence on their time position): 'double' vertices with two dashed tails in Fig.3a, and dashed lines connecting these tails (cf. the examples in Fig.3b). Although 4-, 6- and further $2n$ -fold clusters also form slow ob-

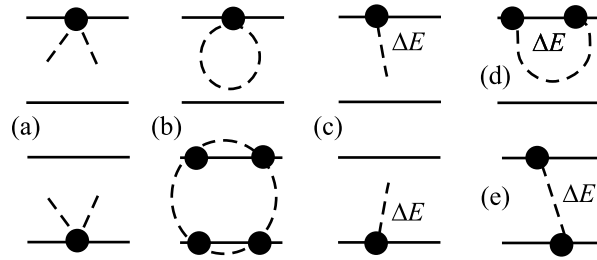


Fig.3. (a) Double vertices with low- ω tails, which appear in the evaluation of dephasing. (b) Examples of clusters built out of them [7]. (c) A low- ω object with a high-frequency dashed line. The relaxation process in (e) also contributes to dephasing as shown in (d)

jects, their creation requires additional constraints on the vertex times (compared to building n pairs) and the respective integration domain is much smaller; thus the contribution of such clusters is of higher order in $\Gamma/\Delta E$.

A closer inspection of the spin dependence and the Keldysh two-branch structure reveals that in each pair both vertices are located on the upper or both on the lower branch (for vertices located on different branches, two terms with different time orderings cancel each other unless the vertices are linked by a dashed line; such a term appears in the analysis of relaxation but not of the dephasing), and they indeed effectively correspond to the term $-Y_2 \sigma_z/2$ in the Hamiltonian.

So far we constructed slow composite objects paying attention only to the oscillations of the solid lines in the diagrams and assuming very slow dashed lines, i.e., neglected the higher-frequency noise. In fact, one can construct another slow object shown in Fig.3c, if the respective oscillations of the solid lines are compensated by the dashed line from this vertex. In other words, in the frequency domain, one constrains the frequency of the dashed line to be ΔE (or $-\Delta E$, depending on the direction of the spin flip at the vertex). The dashed lines from such objects pair up, and the integral w.r.t. their relative position is dominated by small separations, $\delta t \sim 1/\Delta E$. Thus one finds the slow object of Fig.3d, two vertices linked by a dashed line at frequency ΔE ; it describes the relaxational contribution to dephasing $\exp(-t/2T_1)$, where

$$1/T_1 = \zeta^2 S_Y(\Delta E)/2. \quad (7)$$

In similar clusters of higher order additional constraints strongly limit the integration domain. Note that the object in Fig.3d involves the weak noise at a high frequency ΔE , unlike those in Fig.3a, but it is still relevant since the lowest-order term in the upper part of Fig.3b is imaginary and does not contribute to dephasing.

Similarly, we analyze the relaxation of the diagonal entries $\rho_{\uparrow}^{\uparrow}, \rho_{\downarrow}^{\downarrow}$. The new slow ingredient in this analysis is shown in Fig.3e. As for the composite objects in Fig.3a, the terms with these objects located on the upper and lower branches cancel each other, due to different signs ascribed to them in the Keldysh formalism (in contrast, in the analysis of the evolution of $\rho_{\uparrow}^{\uparrow}$ displacing a vertex from one branch to the other flips the spin thus yielding an additional sign change rather than cancellation). Hence the relaxation is given by the terms in Fig.3d,e and Eq. (7). We find that the strong low-frequency noise does not influence the relaxation rate.

Discussion. We focused on the effect of the purely transverse noise. One can verify that in the presence of the longitudinal fluctuations $-\lambda X^2 \sigma_z / 2$ the reduction persists: the relaxation is still given by Eq. (7), and the dephasing can be found by considering the longitudinal noise $-\lambda X^2 + \zeta^2 Y^2 / 2 \Delta E \sigma_z / 2$. For uncorrelated fluctuations $X(t)$ and $Y(t)$ their effects just add up (this would happen in the charge limit $E_C \gg E_J$ for the qubit in Fig.1 at the degeneracy point, where the charge noise is transverse, and at the proper flux bias, where the flux noise is quadratic longitudinal). In the experiment [1] E_C and E_J were comparable, hence both charge and flux noise contributed to longitudinal and transverse fluctuations making them correlated; this should be taken into account but does not complicate the analysis.

We considered slow fluctuations. For short-correlated noise the double vertices of Fig.3a do not contribute, and one recovers the Bloch equations.

Furthermore, we illustrated our analysis by an example of Gaussian noise. Such fluctuations are indeed encountered: The low-frequency noise, e.g. the background-charge fluctuations in Josephson circuits, is possibly produced by a collection of bistable fluctuators (or discrete system with more states). With a proper wide distribution of their parameters (couplings to the qubit, switching rates) they produce a smooth $1/f$ noise power. If the qubit is affected by many fluctuators, with a dense distribution in the parameter space, due to the central limit theorem one expects Gaussian noise. In some Josephson devices sharp noise features indicate that a few fluctuators dominate and the resulting noise is non-Gaussian (dephasing by such fluctuators was studied, e.g., in Ref. [6]). We emphasize that our reduction applies also to the analysis of these systems. Indeed,

our derivation used only the fact that the fluctuations are slow. Thus one can still build the diagrams from the slow objects constructed above but for non-Gaussian fluctuations the dashed tails of the vertices may join not in pairs but also in larger bunches. After the reduction to quadratic longitudinal noise one may use other, non-diagrammatic, ways to analyze its effect.

Our results are relevant for the analysis of the experiment of Ref. [1], in which the measured relaxation and dephasing times were comparable. The prediction of a specific decay law requires a detailed knowledge of the noise power of charge and flux fluctuations. It can be acquired via measurements away from the optimal point, as indicated in Ref. [1].

We thank G. Schön and J. Schrieffer for useful discussions. This work is part of the CFN of the DFG. Y.M. was supported by the Humboldt foundation, the BMBF, and the ZIP programme of the German government.

-
1. D. Vion, A. Aassime, A. Cottet et al., *Science* **296**, 886 (2002).
 2. I. Chiorescu, Y. Nakamura, C. J. P. M. Harmans, and J. E. Mooij, *Science* **299**, 1869 (2003); Y. Yu, S. Han, X. Chu et al., *Science* **296**, 889 (2002); J. M. Martinis, S. Nam, J. Aumentado, and C. Urbina, *Phys. Rev. Lett.* **89**, 117901 (2002); Yu. A. Pashkin, T. Yamamoto, O. Astafiev et al., *Nature* **421**, 823 (2003).
 3. A. Cottet, A. Steinbach, P. Joyez et al., in: *Macroscopic quantum coherence and quantum computing*, Eds. D. V. Averin et al., Kluwer/Plenum, NY, 2001, p. 111.
 4. Y. Nakamura, Yu. A. Pashkin, T. Yamamoto, and J. S. Tsai, *Phys. Rev. Lett.* **88**, 047901 (2002).
 5. A. Shnirman, Yu. Makhlin, and G. Schön, *Phys. Scr.* **T102**, 147 (2002).
 6. E. Paladino, L. Faoro, G. Falci, and R. Fazio, *Phys. Rev. Lett.* **88**, 228304 (2002).
 7. Yu. Makhlin and A. Shnirman, cond-mat/0308297.
 8. Yu. Makhlin, G. Schön, and A. Shnirman, *Rev. Mod. Phys.* **73**, 357 (2001), and references therein.
 9. Y. Nakamura, Yu. A. Pashkin, and J. S. Tsai, *Nature* **398**, 786 (1999).
 10. H. Schoeller and G. Schön, *Phys. Rev.* **B50**, 18436 (1994).
 11. O. V. Konstantinov and V. I. Perel, *ZhETF* **39**, 197 (1961) [*Sov. Phys. JETP* **12**, 142 (1961)].